2013 European Control Conference (ECC)
July 17-19, 2013, Zürich, Switzerland.

Dynamics modeling and comparative robust stability analysis of a space launcher with constrained inputs.

J. Chaudenson, D. Beauvois, S. Bennani, M. Ganet-Schoeller, G. Sandou

Abstract—**This paper presents a comparative robust stability analysis using IQC-based and LMI-based tools. An LFR, resulting from the factorization of the equations of motion, allows assessing the robust stability of a space launcher in the face of inertia uncertainties and saturated inputs.**

I. Introduction

ONE major issue in the field of launcher Guidance Navigation and Control is related to control laws validation in a representative environment. During the atmospheric flight phase, the system is flexible, widely unknown and time-varying (TV) while during the exo-atmospheric flight, the actuator chain is highly nonlinear, the three degrees of freedom dynamic model is coupled and some parameters are uncertain. For this last flight phase, the variety of uncertain parameters and the highly nonlinear behavior of the components cause the analytical validation to be either very complex or based on a non-representative system model. This leads to validation using a time-domain approach based on extensive Monte Carlo simulation [1].

Two main characteristics of the system should be mentioned: first, the dynamic model involves an uncertain inertia matrix and takes into account polynomial gyroscopic couplings. Second, the thruster ON/OFF specific behavior induces a very complex nonlinear actuator modeling. Under these conditions, classical robust stability analysis tools lack precision when modeling the nonlinear or uncertain components. To face this issue, the launcher stability analysis can be split in two parts by dealing with the aforementioned issues separately. In [2], we focused on actuator modeling and assessed robust stability of a system with a simple one dimensional dynamic model. Here, we dwell on the analysis of the three dimensional coupled rotational motion of a space launcher associated with a simple actuator model. Consequently, the dynamic model is considered nonlinear and uncertain, while the actuator model reduces to a saturation operator.

To address the robustness of such systems, the development of stability analysis techniques using Integral Quadratic Constraints (IQC) and Linear Matrix Inequalities (LMI) based methods allows to take into account systems characteristic in a less conservative way and may lead to major improvements in analysis model representativeness. Despite these advances remains the need for an accurate representation of the uncertain nonlinear dynamical system. The aim here is to expose how the equations of motion factorization can lead to a Linear Fractional Representation (LFR) of relatively low dimension, giving a computationally tractable problem. Stability domains are searched with a LMI method in terms of asymptotic stability region and with IQC method in terms of $\mathcal{L}_2$-norm boundedness within a parameter box. This will be done to test the techniques, evaluate the improvements needed to prove stability of an accurate launcher model to fulfill manufacturer needs.

Section II of this paper will review the closed-loop components and section III will introduce the stability analysis methods to be used for robustness assessment. Later, section IV will describe the loop transformation leading to LFR and section V and VI will present the stability results and simulations, respectively.

Notations: n, m are in $\mathbb{N}$; time derivative of signal x is denoted $\dot{x}$; "×" denotes the vector product; I_n, denotes the size n identity matrix; $0_{n\times m}$, denotes the $n \times m$ zero matrix; diag(•) defines diagonal or block diagonal matrices; subscript "i" will denotes the i^{th} row of a vector/matrix.

II. Model Setup

A. Closed-loop overview

Robustness of a representative three degrees of freedom space launcher model controlled by Proportional-Derivative (P-D) control law is assessed (Fig. 1). $\alpha \in \mathbb{R}^3$ represents the launcher actual attitude and subscripts "r" and "e" refer to reference and error; respectively. Signals $\Gamma \in \mathbb{R}^3$ and $\Gamma_d \in \mathbb{R}^3$ are introduced and they represent the torque command and torque delivered by the actuator, respectively. All signals are expressed in the geometrical frame.

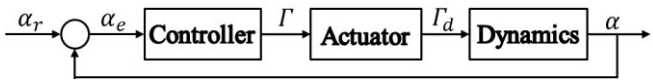

Fig. 1. Closed-loop block diagram with devices and signals to be studied.

The goal of this study is to establish if the nonlinear uncertain closed-loop Fig. 1 is robustly stable when affected by uncertainties of and controlled by constrained inputs.

Manuscript received October 15, 2012. This work was performed in the frame of ESA NPI sponsored PhD for "Nonlinear multivariable analysis techniques for validation of launcher GNC systems", contract n°4000103804.

J. C., D. B. and G. S. are with Supélec, Systems Science (E3S), Automatic Dpt. 3, rue Joliot Curie, 91192 Gif-sur-Yvette. (e-mail: julien.chaudenson@supelec.fr, phone: 00331 69 85 13 84).

S. B. is with ESA/ESTEC (TEC-ECN), Keplerlaan 1, 2201 AZ Noordwijk, the Netherlands. (e-mail: samir.bennani@esa.int).

M. G.-S. is with EADS Astrium S.T., 66 route de Verneuil, 78133 Les Mureaux, France. (e-mail: martine.ganet@eads.astrium.net).

B. Dynamic model and kinematics

Dynamical equation of a rotating rigid body, J_g being the inertia matrix in the geometrical frame, is given in (1). The geometrical frame angular speed with respect to the reference frame is denoted $\omega \in \mathbb{R}^3$. The state variables of the dynamic model are ω and α.

$$\begin{cases} \dot{\omega} = J_g^{-1}\left(\Gamma_d - \omega \times J_g\omega\right) \\ J_g = \begin{bmatrix} J_x & -J_{xy} & -J_{xz} \\ -J_{xy} & J_y & -J_{yz} \\ -J_{xz} & -J_{yz} & J_z \end{bmatrix} \end{cases} \quad (1)$$

In aerospace industry, inertia matrix J_g is always considered to be uncertain when validating control laws to face modeling errors. Diagonal terms of the inertia matrix are in general two orders of magnitude larger than the off-diagonal terms as the launcher tends to be axis symmetric. However, customers are more and more demanding in terms of payload asymmetry so the off-diagonal inertia terms deserve to be investigated for large variation ranges so that inertia specifications could be relaxed.

In this study, we will assume that the launcher attitude α is represented by the angular speed integral instead of Euler angles or quaternions. Nevertheless, we consider that attitude computation does not affect the system stability.

C. Controller and actuator

The controller $\mathcal{C}$ used for attitude tracking has P-D structure with filtered derivative. Its transfer function introduces a filtering factor ω_c common to all axes and control gains K_p and K_d tuned for each axis as if they were decoupled. Transfer function matrix $C(s)$ is diagonal (2). The controller state vector is denoted $x_c \in \mathbb{R}^3$, its input is attitude error α_e and output is Γ. Matrices A_c, B_c, C_c and D_c form its state-space representation.

$$\begin{aligned} C(s) = {} & \mathrm{diag}\left(K_{px}, K_{py}, K_{pz}\right) \\ & + \frac{\omega_c s}{s+\omega_c}\mathrm{diag}\left(K_{dx}, K_{dy}, K_{dz}\right) \end{aligned} \quad (2)$$

The actuator is made of a saturation operator ψ_{u_0}. Saturated ψ_{u_0} outputs (3) are defined by $u_0 \in \mathbb{R}^3$ which is the vector of maximum available torque per axis. The saturation components are defined for all $i \in [\![1;3]\!]$.

$$\left(\psi_{u_0}(y)\right)_i = \begin{cases} y_i, if\ |y_i| < u_{0_i} \\ \mathrm{sign}(y_i) \times u_{0_i}, if\ |y_i| \geq u_{0_i} \end{cases} \quad (3)$$

D. Flight envelope

The space launcher is designed for a certain range of angular speeds and accelerations. This is why we defined a flight envelope in order to limit the angular speed and acceleration values to take into consideration. The purpose of this assumption is to define the flight domain and cover all realistic flight conditions. For the speed, the limit is based on what is usually demanded to the launcher during a mission. Concerning the accelerations, the limits are physical and defined by the attitude control system structure. In facts, the torque produced by the thrusters about each axis is limited and the maximum values are in u_0. Hence, it defines the corresponding maximum nominal acceleration. Of course, the ranges are widened such that launcher never reaches limit speeds and accelerations even for highly coupled cases. The nominal flight envelope is denoted $\mathcal{F}$ and will restrict speed to $\mathcal{F}_\omega$ and acceleration to $\mathcal{F}_{\dot{\omega}}$.

III. Tools For Stability Analysis

A. LMI-based method

To deal with the robust stability analysis, LMI-based methods are efficiently tackling unknown and/or time varying parameters associated with constrained inputs. In this work, we will focus on a method based on the modified sector condition. We will assess the launcher stability by solving LMI using the saturation description proposed in [3]. In order to have an overview of these LMI, we present the result and extend it for parameter varying systems. Initially, it is about linear saturated systems described by (4):

$$\begin{cases} \dot{x} = Ax + B\phi_{u_0}(y) \\ y = Cx \end{cases}, \ x(0) = x_0 \in \mathbb{R}^n \quad (4)$$

where $A \in \mathbb{R}^{n\times n}$, $B \in \mathbb{R}^{n\times m}$ and $C \in \mathbb{R}^{m\times n}$ are the state-space matrices describing the system. The dead-zone function ϕ_{u_0} with output channels defined by the saturation vector u_0 from (3) and for all $i \in [\![1;m]\!]$ by (5).

$$\left(\phi_{u_0}(y)\right)_i = \begin{cases} 0, if\ |y_i| < u_{0_i} \\ y_i - \mathrm{sign}(y_i) \times u_{0_i}, if\ |y_i| \geq u_{0_i} \end{cases} \quad (5)$$

u_0 contains the saturations levels of each channels of the symmetric saturation that were used to define $\mathcal{F}_{\dot{\omega}}$ in II.D. The following theorem ensures asymptotic stability of system (4) inside an ellipsoid of initial conditions.

Theorem: If there exist matrices $W \in \mathbb{R}^{n\times n}$ symmetric positive definite, $S \in \mathbb{R}^{m\times m}$ diagonal positive definite matrix and $Y \in \mathbb{R}^{m\times n}$ such that the LMI conditions:

$$\begin{aligned} &\text{(i)} \ \begin{bmatrix} WA^T + AW & BS + Y^T \\ * & -2S \end{bmatrix} < 0, \\ &\text{(ii)} \ \forall i \in [\![1;m]\!], \begin{bmatrix} W & WC_i^T - Y_i^T \\ * & u_{0_i}^2 \end{bmatrix} \geq 0, \end{aligned} \quad (6)$$

are verified then the ellipsoid $\epsilon(P)$ of (7) with $P = W^{-1}$ is a domain of asymptotic stability for system (4).

$$\epsilon(P) = \{x \in \mathbb{R}^n; x^T P x \leq 1\} \quad (7)$$

If A and B depend on parameters $\theta \in \mathbb{R}^p$ ranging in a polytope with vertices in $\mathcal{V}$, we can check simultaneously the constraints for the state-space representation defined in all $\mathcal{V}$ to ensure robust stability of the well-posed parameter

dependent system as in [4]. Such constraints can be implemented and solved with Matlab®.

B. IQC-based robust stability analysis

IQC approach for robust stability analysis was introduced by [5] as a unifying reformulation of classical input/output theory in an operator-theoretic setting. This method is based on a known nominal LTI system M causal and stable affected by an uncertain system Δ through uncertainty channels (v and w on Fig. 2). Since then, numerous works on IQC analysis [6]-[7] and uncertainties description with multipliers [8]-[9] have been published. For more involved theoretical explanations, the reader may refer to the technical report of the toolbox [10] and [5]. The setting used for stability analysis is given in Fig. 2 where $M(s) = C(sI - A)^{-1}B + D$ is a LTI, causal and stable nominal plant and A, B, C, D are its state-space matrices. Δ is some unknown perturbation operator of an uncertainty set $\mathcal{U}$ consisting of $\mathcal{L}_2$-bounded causal maps.

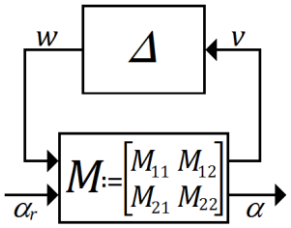

Fig. 2. LFR for IQC analysis, adapted to current problem with Δ perturbation block and M nominal system.

Assuming the operator $I - M_{11}\Delta$ has a causal inverse i.e. the system is well-posed; the system Fig. 2 is stable with uncertainty Δ if the induced $\mathcal{L}_2$-norm (8) of $T = (I - M_{11}\Delta)^{-1}$ is bounded, this norm is defined as:

$$\|T\|_{\mathcal{L}_2 \to \mathcal{L}_2} = \sup_{\substack{w \in \mathcal{L}_2^{n_w} \\ w \neq 0}} \frac{\|Tw\|_2}{\|w\|_2} \tag{8}$$

The notion of IQC is defined using the Fourier transform of finite energy time-domain signals $v \in \mathbb{R}_+ \to \mathbb{R}^{n_v}$ and $w \in \mathbb{R}_+ \to \mathbb{R}^{n_w}$ (Fig. 2), denoted $\hat{v}$ and $\hat{w}$; respectively. Δ is said to be captured by the IQC defined by the multiplier $\Pi : \mathrm{j}\mathbb{R} \to \mathbb{C}^{(n_v+n_w)\times(n_v+n_w)}$ if (9) is verified with $w = \Delta(v)$:

$$\int_{-\infty}^{+\infty} \begin{bmatrix} \hat{v}(j\omega) \\ \hat{w}(j\omega) \end{bmatrix}^* \underbrace{\begin{bmatrix} \Pi_{11}(j\omega) & \Pi_{12}(j\omega) \\ \Pi_{12}(j\omega)^* & \Pi_{22}(j\omega) \end{bmatrix}}_{\Pi(j\omega)} \begin{bmatrix} \hat{v}(j\omega) \\ \hat{w}(j\omega) \end{bmatrix} d\omega \geq 0. \tag{9}$$

For a given $\mathcal{U}$, the set of suitable multipliers Π essentially bounded and Hermitian on the imaginary axis is $\mathcal{M}_{\mathcal{U}}$:

$$\mathcal{M}_{\mathcal{U}} = \left\{ \Pi : \int_{-\infty}^{+\infty} \begin{bmatrix} \hat{v}(j\omega) \\ \tau\hat{w}(j\omega) \end{bmatrix}^* \Pi(j\omega) \begin{bmatrix} \hat{v}(j\omega) \\ \tau\hat{w}(j\omega) \end{bmatrix} d\omega \geq 0, \; \forall \tau \in [0;1], \forall v \in \mathcal{L}_2^{n_v}, w = \Delta(v), \Delta \in \mathcal{U} \right\} \tag{10}$$

and the stability theorem from [5] can be stated.

Theorem: The system Fig. 2 is robustly stable if $I - \tau M_{11}\Delta$ has a causal inverse for all $\tau \in [0;1]$ and there exists $\Pi \in \mathcal{M} \subseteq \mathcal{M}_{\mathcal{U}}$ such that (11) is satisfied:

$$\forall \omega \in \mathbb{R} \cup \{\infty\}, \begin{bmatrix} M_{11}(j\omega) \\ I \end{bmatrix}^* \Pi(j\omega) \begin{bmatrix} M_{11}(j\omega) \\ I \end{bmatrix} < 0. \tag{11}$$

The constraints involved by the theorem can be solved with the Matlab® toolbox [10].

IV. LFR Of The Uncertain Nonlinear Model

A. Dynamics model factorization

The first thing to do is to fit the system in the frameworks of section III in a cost effective fashion and with a representative model. Hence the LFR to be defined needs to cover all feasible trajectories of the launcher and its perturbation matrix to have dimension as low as possible.

For that, we define factorization of (1) to model the uncertain launcher flying within $\mathcal{F}$ by expressing the vector product in the equation of motion (1) as a matrices product (12) introducing speed-dependent skew-symmetric matrix $\Omega(\omega)$ called coupling matrix. A block diagram of the equation of motion is given Fig. 3.

$$\dot{\omega} = J_g^{-1}\left(\Gamma_d - \Omega(\omega) J_g \omega\right) \tag{12}$$

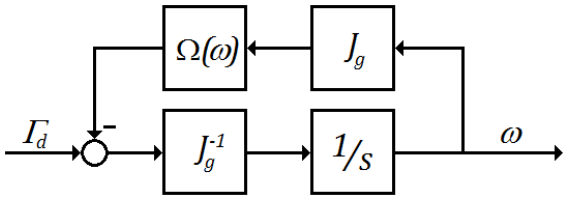

Fig. 3. Block diagram of the equation of motion, s is the Laplace variable, $\Omega(\omega)$ the coupling matrix, J_g the inertia matrix in the geometrical frame.

Secondly, in order to obtain a quasi LPV representation of the system, we define a factorization of matrices J_g and $\Omega(\omega)$ by introducing two diagonal matrices $J_d \in \mathbb{R}^{9\times9}$ with the uncertain terms of J_g and $\Omega_d \in \mathbb{R}^{6\times6}$ with the TV terms of $\Omega(\omega)$ (13). The "hat" notation denotes angular speed components from $\Omega(\omega)$ which are considered as TV parameters. Each term appears as many times as it does in the original matrix so the factorization may not be reducible.

$$\begin{aligned} \forall t \in \mathbb{R}_+, \Omega_d(t) &= \mathrm{diag}(\hat{\omega}_z(t)I_2, \hat{\omega}_y(t)I_2, \hat{\omega}_x(t)I_2) \\ J_d &= \mathrm{diag}(J_x, J_y, J_z, J_{xy}I_2, J_{xz}I_2, J_{yz}I_2) \end{aligned} \tag{13}$$

Finally, J_d and Ω_d are associated to placement matrices M_1, M_2^T in $\mathbb{R}^{3\times9}$ and T_1, T_2^T in $\mathbb{R}^{3\times6}$ to give the factorized expressions of J_g and $\Omega(\omega)$ of (14).

$$\begin{cases}\Omega(\omega) = T_1\Omega_d T_2 \\ J_g = M_1 J_d M_2\end{cases}$$

with

$$M_1 = \begin{bmatrix}1&0&0&1&0&1&0&0&0\\0&1&0&0&1&0&0&1&0\\0&0&1&0&0&0&1&0&1\end{bmatrix}, \quad (14)$$

$$M_2 = \begin{bmatrix}1&0&0&0&-1&0&-1&0&0\\0&1&0&-1&0&0&0&0&-1\\0&0&1&0&0&-1&0&-1&0\end{bmatrix}^T,$$

$$T_1 = \begin{bmatrix}1&0&1&0&0&0\\0&1&0&0&1&0\\0&0&0&1&0&1\end{bmatrix} \text{ and } T_2 = \begin{bmatrix}0&1&0&-1&0&0\\-1&0&0&0&0&1\\0&0&1&0&-1&0\end{bmatrix}^T$$

B. LFR of the dynamics

Considering definitions (14), the last step to build the LFR is to introduce the uncertainties on the terms of J_d and Ω_d. We consider the inertia terms to be affected by direct multiplicative relative uncertainty and introduce the uncertain inertia matrix Δ_J. The coupling matrix is assumed to be affected by additive uncertainty. The resulting expressions for Ω_d and J_d are presented in (15) with J_{d0} and Ω_{d0} consisting of nominal values of J_d and Ω_d, respectively.

$$\begin{cases}J_d = J_{d0}(I_9 + \Delta_J) \\ \Omega_d = \Omega_{d0} + \Delta_\omega\end{cases} \quad (15)$$

Finally, expressions of J_g and $\Omega(\omega)$ are expanded to give their LFR expressions (16). These equations result in the block diagram Fig. 4, defining the dynamic model LFR.

$$\begin{cases}J_g = J_{g_0}\left(I_3 + J_{g0}^{-1}M_1 J_{d0}\Delta_J M_2\right) \text{ with } J_{g_0} = M_1 J_{d0} M_2 \\ \Omega(\omega) = \Omega_0 + T_1\Delta_\omega T_2 \text{ with } \Omega_0 = T_1\Omega_{d0}T_2\end{cases} \quad (16)$$

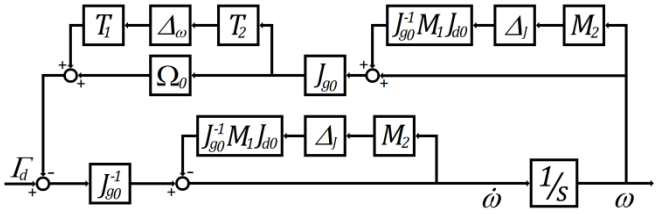

Fig. 4. LFR of the uncertain factorized equations of motion.

C. LFR of the actuator

For robustness analysis, saturations are usually represented with a unit gain and a dead-zone (5) as in Fig. 5. LMI method from III.A. relies on such a transformation and uses the modified sector condition to represent fully the dead-zone behavior. Model Fig. 5 is also appropriate to IQC method. However, the IQC tool models the dead-zone operator as a memoryless non linearity in a sector. It causes the model to be singular along sector $\{0;1\}$ border. This particular case has been investigated in [11] but will not be taken into account here. To avoid singularity we will consider the dead-zone operator to be in a sector $\{0;1-\epsilon\}$, $0 < \epsilon \ll 1$, and check during the simulation that (17) is satisfied for all $t \in \mathbb{R}_+$.

$$\forall i \in [\![1;3]\!], |\Gamma_i(t)| < \Gamma_{\max_i} = u_{0_i}/\epsilon \quad (17)$$

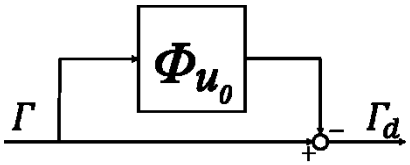

Fig. 5. LFR for the saturation is defined with dead-zone operator to deliver the constrained torque Γ_d.

D. Closed-loop LFR

To conclude this section the closed-loop LFR state-space representation is defined by its signals (18), perturbation block (19) and matrices (20). As we have a repetition of operator Δ_J in the LFR, corresponding input and output channels are labeled by subscripts "1" and "2". Other subscripts "ω" and "sat" are for the TV speed parameters and the dead-zone operator; respectively.

$$\begin{aligned}&\text{State vector: } x = [\omega \quad \alpha \quad x_c]^T \in \mathbb{R}^9 \\ &\text{Input vector: } w = [w_{J_1} \quad w_{J_2} \quad w_\omega \quad w_{sat}]^T \in \mathbb{R}^{27} \\ &\text{Output vector: } v = [v_{J_1} \quad v_{J_2} \quad v_\omega \quad v_{sat}]^T \in \mathbb{R}^{27}\end{aligned} \quad (18)$$

Performance input/output channels are void for stability assessment and state matrices of $M = M_{11}$ (Fig. 2.) are denoted A, B, C, D in (20) and the relationship between v and w is $w = \bar{\Delta}v$ using perturbation operator $\bar{\Delta}$ in (19).

$$\bar{\Delta} = \text{diag}\left(\Delta_J, \Delta_J, \Delta_\omega, \phi_{u_0}(\bullet)\right) \quad (19)$$

$$A = \begin{bmatrix}-J_{g0}^{-1}\Omega_0 J_{g0} & -J_{g0}^{-1}D_c & J_{g0}^{-1}C_c \\ I_3 & 0_{3\times3} & 0_{3\times3} \\ 0_{3\times3} & -B_c & A_c\end{bmatrix},$$

$$B = [B_u \quad B_{nl}], C = \begin{bmatrix}C_u \\ C_{nl}\end{bmatrix}, D = \begin{bmatrix}D_{u,u} & D_{u,nl} \\ 0_{3\times24} & 0_{3\times3}\end{bmatrix},$$

$$B_u = \begin{bmatrix}-J_{g0}^{-1}\Omega_0 M_1 J_{d0} & -J_{g0}^{-1}M_1 J_{d0} & -J_{g0}^{-1}T_1 \\ 0_{3\times9} & 0_{3\times9} & 0_{3\times6} \\ 0_{3\times9} & 0_{3\times9} & 0_{3\times6}\end{bmatrix},$$

$$B_{nl} = \begin{bmatrix}-J_{g0}^{-1} \\ 0_{3\times3} \\ 0_{3\times3}\end{bmatrix}, C_u = \begin{bmatrix}M_2 & 0_{9\times3} & 0_{9\times3} \\ -M_2 J_{g0}^{-1}\Omega_0 J_{d0} & -M_2 J_{g0}^{-1}D_c & M_2 J_{g0}^{-1}C_c \\ T_2 J_{g0} & 0_{6\times3} & 0_{6\times3}\end{bmatrix},$$

$$C_{nl} = [0_{3\times3} \quad -B_c \quad A_c], \quad D_{u,nl} = \begin{bmatrix}0_{9\times3} \\ -M_2 J_{g0}^{-1} \\ 0_{6\times3}\end{bmatrix} \text{ and}$$

$$D_{u,u} = \begin{bmatrix}0_{9\times9} & 0_{9\times9} & 0_{9\times6} \\ -M_2 J_{g0}^{-1}\Omega_0 M_1 J_{d0} & -M_2 J_{g0}^{-1}M_1 J_{d0} & -M_2 J_{g0}^{-1}T_1 \\ T_2 M_1 J_{d0} & 0_{6\times9} & 0_{6\times6}\end{bmatrix} \quad (20)$$

The above definition does not group the channels affected by the same scalar uncertainty on inertias. Before proceeding to the robustness analysis, input/output vectors are reorganized such that signals affected by the same uncertainty are grouped together in perturbation matrix $\Delta = \text{diag}(\Delta_u, \Delta_{nl})$ with Δ_u defined in (21) while $\Delta_{nl} = \phi_{u_0}$.

$$\Delta_u = \text{diag}\left(\delta_{Jx}I_2, \delta_{Jy}I_2, \delta_{Jz}I_2, \delta_{Jxy}I_4, \delta_{Jxz}I_4, \delta_{Jyz}I_4, \Delta_\omega\right) \quad (21)$$

V. Stability Analysis

A. Introduction

The LMI based method needs the state-space representation to be recast while the IQC-based method can be used directly on the model defined in IV.D. We consider the diagonal inertia terms to be uncertain to $\pm 10\%$ and off-diagonal terms to be multiplied by an unknown factor between 0 and 10 while speeds and accelerations are considered to be ranging in the nominal flight envelope $\mathcal{F}$.

B. LMI-based method

The first step of the analysis is to evaluate the state-space representation of the system at the vertices of the parameters box. From the state-space representation (18)-(19)-(20), we can build a representation separating outputs linked to uncertainty channels to those linked to nonlinearities channels. Thus we split the state-space matrices of (20) and write $w = [w_u \quad w_{nl}]^T$ and $v = [v_u \quad v_{nl}]^T$ to obtain

$$\begin{cases} \dot{x} = Ax + B_u w_u + B_{nl} w_{nl} \\ v_u = C_u x + D_{u,u} w_u + D_{u,nl} w_{nl} \\ v_{nl} = C_{nl} x \\ w_u = \Delta_u v_u \end{cases} \tag{22}$$

which can be reduced to the form (23) similar to (4):

$$\begin{cases} \dot{x} = \mathcal{A}x + \mathcal{B} w_{nl} \\ v_{nl} = C_{nl} x \end{cases} \tag{23}$$

with

$$\begin{cases} \mathcal{A} = A + B_u \Delta_u \left(I_{24} - D_{u,u}\Delta_u\right)^{-1} C_u \\ \mathcal{B} = B_{nl} + B_u \Delta_u \left(I_{24} - D_{u,u}\Delta_u\right)^{-1} D_{u,nl} \end{cases} \tag{24}$$

The LFR is well-posed and has $p = 9$ uncertain parameters ranging in a rectangle. It results in the definition of a set of 2^p system vertices $\mathcal{K} := \{(\mathcal{A}_k, \mathcal{B}_k), k \in [\![1; 2^p]\!]\}$ in the state-space. According to [4], we test the LMI constraints (6) feasibility for the 75 decision variables at all vertices of the parameters box to ensure stability in the convex hull of $\mathcal{K}$.

For the nominal flight envelope $\mathcal{F}$, the constraints are not feasible and so $\epsilon(P)$ cannot be defined. To be able to define an ellipsoid of asymptotic stability, we reduced the range of angular speeds $\mathcal{F}_\omega$ while keeping acceleration ranges $\mathcal{F}_{\dot{\omega}}$ at their nominal value. The LMI constraints became feasible when multiplying the speed ranges by 0.54, forming reduced flight envelope $\mathcal{F}'$. Asymptotic stability is proved for initial conditions in $\epsilon(P) \cap \mathcal{F}_\omega$ as presented in Fig. 6.

The conservatism of this method is due to the search of quadratic stability over the whole parameters set without taking into account the parameter characteristics such as time-invariance and/or limitation on derivatives for time-varying parameters. Hence the search of a quadratic Lyapunov function with constant matrix is too conservative to cope with nine unknown parameters as it covers the case of time-varying parameters varying arbitrarily fast. Nevertheless, the dead-zone is completely captured by the modified sector condition [3] ensuring rigorous results.

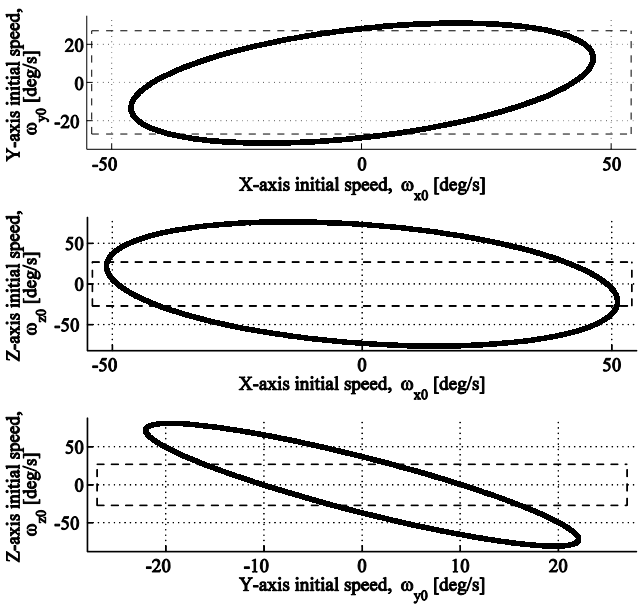

Fig. 6. Projections on speed planes of the region of asymptotic stability defined by $\epsilon(P) \cap \mathcal{F}'$; $\mathcal{F}'_\omega$: dashed line (--) and $\epsilon(P)$: thick line (–). Inertia uncertainties are from V.A. and the reduced flight envelope is $\mathcal{F}'$ with $\mathcal{F}'_\omega = 0.54 \times \mathcal{F}_\omega$.

C. IQC-based method

The launcher robustness is evaluated with the IQC tool presented in [10]. To capture the saturation defined with the odd-monotone nonlinear dead-zone operator, the Zames-Falb multiplier [12] is used. The maximum gain ($\beta = 1 - \epsilon$ with $\epsilon = 1 \times 10^{-3}$) and maximum incremental gain ($\mu = 1$) of the dead-zone. Multipliers for inertia uncertainty are defined as constant scalings adaptations from [13] while those defining the IQC which captures the TV speed parameters are defined using data from both $\mathcal{F}_\omega$ and $\mathcal{F}_{\dot{\omega}}$ following the method in [14]. To choose the poles of the multipliers for the dead-zone and the TV parameters, we searched over a grid of values. We did not consider any link between these poles and selected independently the values giving the largest stability domain.

IQC-based method proves stability over $\mathcal{F}$ and for aforementioned inertia uncertainties in a basic configuration with small problem size and so small computational burden. Even in this simple context, it leads to less conservative results for mixed perturbations in comparison with LMI method. It should also be noticed that we used low order multipliers for this problem and that conservatism can be reduced by increasing their order or tuning their pole values in a more rigorous fashion than during this study.

VI. Simulations

In the frame of this study, we also need to assess the launcher behavior in the stability domain. To do so, we perform a despin maneuver simulation. It aims to reduce the roll axis angular speed from $20\ \mathrm{deg.s^{-1}}$ down to $0\ \mathrm{deg.s^{-1}}$ keeping transverse axes stabilized. Quaternions are taken into for the simulations and we invite the reader to refer to

[15] for information on the topic. Angular speeds are plotted in Fig. 7 for the same maneuver with 500 different inertia parameters combinations among which the vertices of the inertia parameter box. It is clear that if the launcher seems to follow the reference speed, large perturbations and long transient motion appear on the transverses axes for some inertia combinations. Moreover, the speeds are taking several minutes to get back within precision bounds which are usually under $1\ \mathrm{deg.s^{-1}}$. The simulations show that IQC stability criterion should be reinforced with performance constraints to satisfy the manufacturer's performance needs.

Finally, we observed that, in this configuration with widely unknown parameters, none of the constraints we introduced during the modeling phase, $\mathcal{F}$ and (17), have been violated.

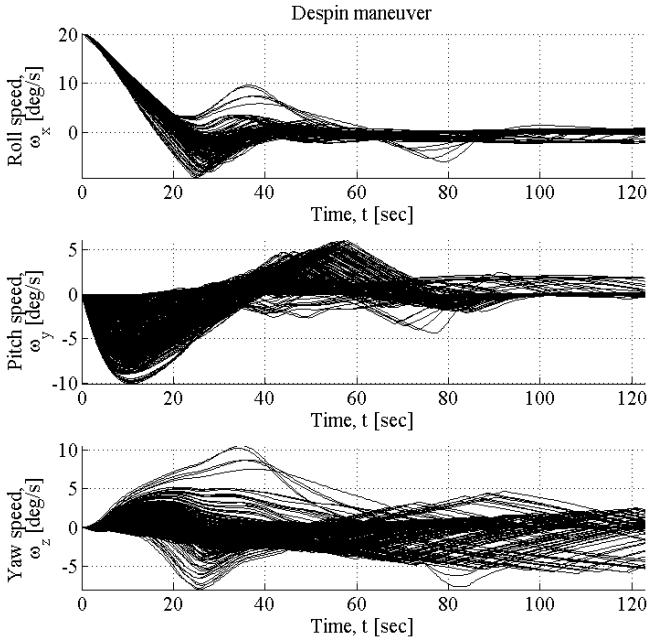

Fig. 7. Angular speeds for 500 simulations at vertices of the stability domain and with random inertias within the stability domain obtained with the IQC tool.

VII. CONCLUSIONS

The modeling step in this work presents a compact factorization for the equations of motion of a rotating rigid body. This representation has two main assets. First it seems to be not reducible and represents all inertia parameters. The low dimension of the perturbation matrix gives possibilities for an increase of model representativeness. Second, the uncertain inertia parameters represent actual inertia variations leading to a better understanding.

The comparative robustness analysis showed the capability of IQC methods to assess stability of complex systems. Indeed, the LMI method based on the modified sector condition is dedicated to and efficient for analysis of constrained systems. However, the search for the ellipsoid of asymptotic stability when the system is uncertain is too conservative with our method based on the search of a constant Lyapunov matrix. On the contrary, the IQC-based method addressed the problem with time-varying parameters, uncertain constant parameters and a nonlinearity dealing with them using a dedicated multiplier for each one of the perturbations and concluding to $\mathcal{L}_2$-boundedness of the system. Computation durations are comparable of about 15 minutes for each feasibility test.

Nevertheless, time-simulations showed that the IQC criterion of $\mathcal{L}_2$-stability is not strong enough to guarantee a satisfying behavior of the launcher over the whole flight domain. In facts the performances are poor in some cases and further works will focus on including performance weightings in the IQC analysis such that it will ensure manufacturers performance criteria to be fulfilled.

REFERENCES

[1] J-W. Jang, C. Van Tassel, N. Bedrossian, C. Hall, P. Spanos, Evaluation of ARES I control system robustness to uncertain aerodynamics and flex dynamics. *AIAA GNC Conf.*, 2008-6621, 2008.

[2] J. Chaudenson. D. Beauvois. S. Bennani. C. Frechin. M. Ganet-Schoeller. G. Sandou. C.W. Scherer., PWM modeling for attitude control of a launcher during ballistic phase and comparative stability analysis. *In Proceedings of the* 7th *IFAC ROCOND*, Aalborg, Denmark, June, 2012.

[3] J.M. Biannic, S. Tarbouriech, and D. Farret. A practical approach to performance analysis of saturated systems with application to fighter aircraft controllers. *In Proceedings of the* 5th *IFAC ROCOND*, Toulouse, France, July, 2006.

[4] S. Boyd and Q. Yang, Structured and simultaneous Lyapunov functions for system stability problems, *Int. Journal of Control*, 49(6):2215-2240, 1989.

[5] Megretski, A. Rantzer, System analysis via integral quadratic constraints, *IEEE Trans. on Aut. Control*, **42-6**, pp 819-830, 1997.

[6] H. Fujioka, K. Morimura, Computational aspects of IQC-based stability analysis for sampled-data feedback systems. *38th IEEE CDC*, pp 3452-3457, 1999.

[7] Y-C. Chu, K. Glover, A.P. Dowling, Control of combustion oscillations via $\mathcal{H}_\infty$ loop-shaping, μ-analysis and IQC. *Automatica*, **39**, pp 219-231, 2003.

[8] Helmersson, An IQC-based stability criterion for systems with slowly varying parameters. Technical report, Dpt. of Electrical Engineering, Linköping university, 1999.

[9] C-Y. Kao, A. Rantzer, Stability criteria for systems with bounded uncertain time-varying delay. *ECC*, pp 1578-1583, 2003.

[10] C.W. Scherer, H. Köroglu, M. Farhood, *LPVMAD – The IQC analysis tool*. Tech. report, TU Delft for ESA, 2008.

[11] D. Peaucelle, S. Tarbouriech, M. Ganet-Schoeller, S. Bennani. Evaluating regions of attraction of LTI systems with saturations in IQS framework. *In Proceedings of the* 7th *IFAC ROCOND*, Aalborg, Denmark, June, 2012.

[12] G. Zames, P. L. Falb, Stability conditions for systems with monotone and slope-restricted non-linearities, *SIAM Journal on Control*, **6-1**, pp 89-108, 1968.

[13] M.K.H. Fan, A.L. Tits, J.C. Doyle, Robustness in the presence of mixed-parametric uncertainty and unmodeled dynamics, *IEEE Trans. on Aut. Control*, Vol.36, No.1, pp 25-38, 1991.

[14] H. Köroglu, C.W. Scherer, Robust stability analysis against perturbations of smoothly time-varying parameters, *In Proceedings of IEEE Conference on Decision and Control*, pp.2895-2900, San Diego, CA, 2006.

[15] M.J. Sidi, Spacecraft dynamics and control, Cambridge Aerospace Series, Ed. M. J. Rycroft & R. F. Stengel, 1997.